

# Algorithm Refinement for Stochastic Partial Differential Equations

## I. Linear Diffusion

Francis J. Alexander,<sup>\*</sup> Alejandro L. Garcia,<sup>†,1</sup> and Daniel M. Tartakovsky<sup>‡</sup>

<sup>\*</sup>CCS-3, Los Alamos National Laboratory, Los Alamos, New Mexico 87545; <sup>†</sup>Center for Applied Scientific Computing, Lawrence Livermore National Laboratory, Livermore, California 94551; and <sup>‡</sup>T-7, Los Alamos National Laboratory, Los Alamos, New Mexico 87545

E-mail: fja@lanl.gov

Received October 29, 2001; revised May 29, 2002

---

A hybrid particle/continuum algorithm is formulated for Fickian diffusion in the fluctuating hydrodynamic limit. The particles are taken as independent random walkers; the fluctuating diffusion equation is solved by finite differences with deterministic and white-noise fluxes. At the interface between the particle and continuum computations the coupling is by flux matching, giving exact mass conservation. This methodology is an extension of Adaptive Mesh and Algorithm Refinement to stochastic partial differential equations. Results from a variety of numerical experiments are presented for both steady and time-dependent scenarios. In all cases the mean and variance of density are captured correctly by the stochastic hybrid algorithm. For a nonstochastic version (i.e., using only deterministic continuum fluxes) the mean density is correct, but the variance is reduced except in particle regions away from the interface. Extensions of the methodology to fluid mechanics applications are discussed. © 2002 Elsevier Science (USA)

---

## 1. INTRODUCTION

Numerical modeling of complex systems has benefited tremendously from recent advances in both computational power and algorithm sophistication. However, for a very important and growing class of so-called multiscale (space and/or time) applications, hardware developments alone will not be sufficient. Moreover, conventional, single-method algorithmic approaches will simply be unable to capture the relevant phenomena occurring over the many space and time scales.

<sup>1</sup> Permanent address: Dept. of Physics, San Jose State Univ., San Jose, CA 95192-0106.

An efficient approach for multiscale problems is to perform detailed calculations, using an expensive algorithm, only where absolutely required and to couple this computation to a simpler, less expensive method, which is used in the rest of the domain. Such “hybrid” methods typically couple (at least) two structurally (physically and algorithmically) different computational schemes, which are used in different regions of the problem (e.g., interior and exterior of a shock wave). One class of hybrids involves matching particle methods to continuum partial differential equation (PDE) solvers [1–12]; other hybrids combine stochastic systems with deterministic ones, explicit schemes with implicit ones, etc.

This multi-algorithm approach, also known as Algorithm Refinement, is advantageous when the computational expense of a hybrid calculation is much less than that of performing the entire calculation using the more expensive of the two algorithms. Assuming that the computational cost increases linearly with physical volume, which is typical for explicit methods, this criterion can be expressed as

$$V_1 C_1 + V_2 C_2 + V_{\leftrightarrow} C_{\leftrightarrow} \ll V C_1,$$

where  $C_1$ ,  $C_2$ , and  $C_{\leftrightarrow}$  are the computational cost per unit volume for each algorithm ( $C_1 \gg C_2$ ) and for the interface region between the two methods, respectively;  $V_1$ ,  $V_2$ , and  $V_{\leftrightarrow}$  are the respective volumes modeled by each method, and  $V$  is the total physical volume ( $V_1 + V_2 \leq V \leq V_1 + V_2 + V_{\leftrightarrow}$ ). This criterion is approximately

$$\frac{V_{\leftrightarrow}}{V - V_1} \frac{C_{\leftrightarrow}}{C_1} \ll 1.$$

We see the benefit of a hybrid even if the algorithmic interface is computationally more expensive than either algorithm, as long as the interface region and the region using the more expensive method are each small fractions of the total volume.

An important question is whether (and how) the coupling of two algorithms affects the accuracy of either method. Until now, the testing of Algorithm Refinement schemes has focused on mean values such as average density, temperature, etc. Yet for simulations of microscopic systems, one is also interested in the variations of these quantities due to spontaneous fluctuations. This is likely to be important for modeling phenomena where the fluctuations themselves drive (or initiate) a large-scale process, such as the onset of instabilities and the nucleation of phase transitions.

In this paper we address the issue of fluctuations in hybrid schemes, specifically those schemes that combine a particle algorithm with a partial differential equation solver. Since our interest is in fluctuations, we consider both deterministic and stochastic partial differential equations. Our investigation focuses on the problem of simple diffusion since much is known about solving the linear diffusion equation (LDE) in both its deterministic and stochastic forms. Moreover, there is a microscopic particle process, namely independent random walkers, which rigorously converges to the LDE in the hydrodynamic scaling limit. Thus we have an ideal testbed for investigation.

In Section 2 we comment on the random walk model and the linear diffusion equation (LDE) including its stochastic form. In Section 3 we describe numerical schemes for simulating this model and for computing this stochastic PDE. Following that, in Section 4 we discuss ways to couple these two very different representations. Section 5 presents the results of our numerical investigations, and Section 6 describes a way to analyze systems that couple stochastic and deterministic components. We close in Section 7 with a discussion of our results and a list of further directions.

## 2. SIMPLE DIFFUSION: PARTICLE AND CONTINUUM THEORIES

Consider the well-known random walk model. Specifically, take a system of  $N$  independent (i.e., noninteracting) particles that evolve according to the stochastic dynamics

$$dX_k(t) = DdW_k, \quad (1)$$

where  $X_k$  is the location of particle  $k$ ,  $D$  is the diffusion constant, and  $W$  is a standard Wiener process [13].

Define the density of particles in a region

$$\rho(x, t) = \sum_{k=1}^N \delta(x - X_k(t)). \quad (2)$$

The Fokker–Planck equation for the random walker dynamics, in the hydrodynamic limit, yields the one-dimensional, fluctuating diffusion equation [13]

$$\frac{\partial \rho}{\partial t} = -\frac{\partial F}{\partial x} = D \frac{\partial^2}{\partial x^2} \rho - \frac{\partial f}{\partial x}, \quad (3)$$

where  $F$  is the total particle flux, whose deterministic component is given by Fick's law,  $-D\partial\rho/\partial x$ . Its fluctuating component,  $f$ , is a Gaussian white noise with zero mean and correlation

$$\langle f(x, t)f(x', t') \rangle = A(x, t)\delta(x - x')\delta(t - t'), \quad (4)$$

where the angle brackets indicate an ensemble average. The noise amplitude,  $A(x, t)$ , is related to the equal-time correlation of density fluctuations, which is taken to be

$$G(x, x') = \langle \delta\rho(x, t)\delta\rho(x', t) \rangle = \bar{\rho}(x, t)\delta(x - x') + C, \quad (5)$$

where  $\delta\rho = \rho - \bar{\rho}$ , and the deterministic density is given by the solution of

$$\frac{\partial \bar{\rho}}{\partial t} = D \frac{\partial^2 \bar{\rho}}{\partial x^2}, \quad (6)$$

with the same initial and boundary conditions as (3). For an open system (a system in contact with a particle or density reservoir), the constant  $C = 0$ ; for a closed system of length  $L$ ,

$$C = -\frac{N}{L^2}; \quad N = \int_0^L \rho(x, t) dx = \int_0^L \bar{\rho}(x, t) dx, \quad (7)$$

due to mass conservation. Given (5), the noise amplitude is [13]

$$A = 2D\bar{\rho}(x, t). \quad (8)$$

Note that for open systems the variance in the number of particles within an interval equals the mean number in that interval, as with the Poisson distribution; for closed systems the variance is reduced due to mass conservation.

### 3. SIMPLE DIFFUSION: PARTICLE AND CONTINUUM ALGORITHMS

The numerical simulation of the random walk model is straightforward: intergrating both sides of (1) over a time increment  $\Delta t$  yields

$$X_k(t + \Delta t) - X_k(t) = \sqrt{2D\Delta t} \mathfrak{R}_k, \quad (9)$$

where  $\mathfrak{R}_k$  are independent, Gaussian-distributed random values with zero mean and unit variance. At each time step every walker is given a random displacement, as in Eq. (9).

If we discretize space and time in the continuum formulation, we may write the stochastic diffusion equation, (3), as

$$\frac{\rho_{i;n+1} - \rho_{i;n}}{\Delta t} = - \left( \frac{F_{i;n}^+ - F_{i;n}^-}{\Delta x} \right), \quad (10)$$

where  $\rho_{i;n} = \rho(x_i, t_n)$  with  $x_i = (i - \frac{1}{2})\Delta x$ ,  $i = 1, \dots, M$ , and  $t_n = n\Delta t$ ,  $n = 0, 1, \dots$ . The discretized fluxes (right and left) are

$$F_{i;n}^\pm = \mp D \left( \frac{\rho_{i\pm 1;n} - \rho_{i;n}}{\Delta x} \right) + f_{i;n}^\pm. \quad (11)$$

The discretized correlation of the fluctuating particle flux may be written as [14]

$$\langle f_{i;n}^+ f_{j;m}^+ \rangle = \frac{(A_{i;n} + A_{i+1;n})\delta_{i,j}\delta_{n,m}}{2\Delta x \Delta t}; \quad \langle f_{i;n}^- f_{j;m}^- \rangle = \frac{(A_{i;n} + A_{i-1;n})\delta_{i,j}\delta_{n,m}}{2\Delta x \Delta t}, \quad (12)$$

and  $F_{i;n}^+ = F_{i+1;n}^-$ , so

$$f_{i;n}^+ = f_{i+1;n}^- = \frac{\sqrt{(A_{i;n} + A_{i+1;n})}}{2\Delta x \Delta t} \mathfrak{R}_{i;n}, \quad (13)$$

where  $\mathfrak{R}_{i;n}$  are independent, Gaussian-distributed, random variables with zero mean and unit variance.

Collecting the above yields a Langevin-type numerical scheme for the density,

$$\begin{aligned} \rho_{i;n+1} = \rho_{i;n} + \frac{D\Delta t}{\Delta x^2} (\rho_{i+1;n} + \rho_{i-1;n} - 2\rho_{i;n}) \\ - \sqrt{\frac{D\Delta t}{\Delta x^3}} (\sqrt{\bar{\rho}_{i;n} + \bar{\rho}_{i+1;n}} \mathfrak{R}_{i;n} - \sqrt{\bar{\rho}_{i;n} + \bar{\rho}_{i-1;n}} \mathfrak{R}_{i-1;n}), \end{aligned} \quad (14)$$

since  $A_{i;n} = 2D\bar{\rho}_{i;n}$ .

This scheme is essentially the same as that presented in reference [14] for the Fourier (heat) equation except for the form of the noise amplitude. For mass diffusion the amplitude is linear in the density while for temperature diffusion it is quadratic in the temperature, which leads to long-ranged spatial correlations of equal-time fluctuations [14–16].

Using (14), the equal-time correlation function  $G_{i,j} \equiv \langle \delta\rho_{i;n}\delta\rho_{j;n} \rangle$  is

$$\begin{aligned} & 4\left(1 - \frac{D\Delta t}{\Delta x^2}\right)G_{i,j} - \left(1 - \frac{2D\Delta t}{\Delta x^2}\right)(G_{i,j+1} + G_{i,j-1} + G_{i+1,j} + G_{i-1,j}) \\ & \quad - \frac{D\Delta t}{\Delta x^2}(G_{i+1,j+1} + G_{i+1,j-1} + G_{i-1,j+1} + G_{i-1,j-1}) \\ & = \frac{1}{\Delta x}(B_i B_j \delta_{i,j} - B_i B_{j-1} \delta_{i,j-1} - B_{i-1} B_j \delta_{i-1,j} + B_{i-1} B_{j-1} \delta_{i-1,j-1}), \end{aligned} \quad (15)$$

where  $B_i = \sqrt{\bar{\rho}_{i;n} + \bar{\rho}_{i+1;n}}$ . Note that if the deterministic density is linear (i.e.,  $\bar{\rho}_{i+1;n} - \bar{\rho}_{i;n}$  is independent of  $i$ ), then

$$\begin{aligned} & B_i B_j \delta_{i,j} - B_i B_{j-1} \delta_{i,j-1} - B_{i-1} B_j \delta_{i-1,j} + B_{i-1} B_{j-1} \delta_{i-1,j-1} \\ & = 4\bar{\rho}_{i;n} \delta_{i,j} - (\bar{\rho}_{i;n} \delta_{i,j+1} + \bar{\rho}_{i;n} \delta_{i,j-1} + \bar{\rho}_{i+1;n} \delta_{i+1,j} + \bar{\rho}_{i-1;n} \delta_{i-1,j}). \end{aligned} \quad (16)$$

In the limit  $\Delta t \rightarrow 0$ , the static correlation is

$$G_{i,j} = \frac{\bar{\rho}_{i;n}}{\Delta x} \delta_{i,j} + C, \quad (17)$$

in agreement with the continuum result, Eq. (5).

The above formulation is somewhat cumbersome in that the deterministic PDE (6) must be evaluated separately to obtain the space- and time-dependent  $\bar{\rho}$ , since the noise amplitude is  $A = 2D\bar{\rho}$ . For the linear, stochastic diffusion equation we may extend the additive noise to be multiplicative, that is,  $A = 2D\rho(x, t)$ , in the limit where the fluctuations about the mean are small [17]. In the discrete numerical scheme, (14), we may replace  $\bar{\rho}_{i;n}$  with  $\rho_{i;n}$  in the noise terms; this generalization is tested and validated by the numerical simulations in Section 5.

#### 4. PARTICLE/CONTINUUM HYBRID ALGORITHM

Having presented the stochastic PDE corresponding to independent, random walk particle dynamics and outlined the numerical schemes for each representation (particle and continuum), we now describe how to couple the two numerical methods. Figure 1 illustrates a typical hybrid calculation with a particle region within the interval from  $x = 0$  to  $I$ ; elsewhere the continuum density is specified at discrete grid points. For the purpose of statistical measurements and plotting *only*, the density in the particle regions is evaluated

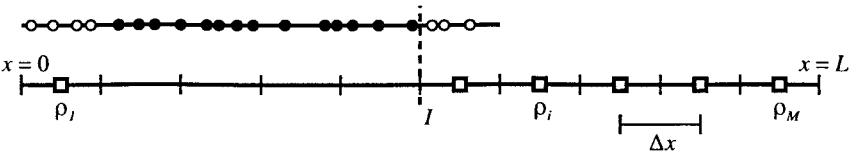


**FIG. 1.** Algorithm Refinement for simple diffusion. A random walk simulation is performed in the region on the left and a PDE solver is used on the right. The methods are coupled at the interface  $I$ ; new particles (open circles) are generated in the “handshaking” region (right) and at the Dirichlet boundary (left).

on the same grid as the discretized continuum calculation. Specifically,

$$\rho_{i;n} = \frac{1}{\Delta x} \sum_{k=1}^N \delta \left[ x_i - \frac{1}{2} \Delta x < X_{k;n} < x_i + \frac{1}{2} \Delta x \right], \quad (18)$$

where  $X_{k;n}$  is the position of particle  $k$  at time  $t = n \Delta t$ ; the boolean delta function is defined as  $\delta[A] = 1$  if  $A$  is true, and  $= 0$  otherwise. Initially, a density is assigned to all  $M$  grid points, and particles are generated within the particle region. For steady-state problems, the specific initialization process does not affect the final answer. For investigation of time-dependent phenomena, of course, the initial distribution is relevant and will be described in detail in the following section.

At the beginning of a time step, the particle region is extended by one grid point into the continuum region. This added ‘‘handshaking’’ region is uniformly filled with  $N_{i;n}$  particles according to the density of the underlying grid point, taking  $N_{i;n} = \rho_{i;n} \Delta x$ , rounded to an integer. Other ways of filling the region were tested (nonuniform distribution of particle positions using  $\nabla \rho$ , Poisson distribution for  $N_{i;n}$  with mean  $\rho_{i;n} \Delta x$ , etc.) but were found to give equal or poorer results. All particles, in the handshaking region and elsewhere, are then displaced as  $X_{k;n+1} = X_{k;n} + \delta X_{k;n}$ , where the distance  $\delta X_{k;n} = \sqrt{2D\Delta t} \mathfrak{R}_{k;n}$  (see Eq. (9)). The number of particles crossing the interface gives the number flux at  $I$ ; this flux is recorded and used in the continuum portion of the computation (see below). Any particles that end their move outside the particle region are removed from the simulation.

Once the particle update is complete, (11) is used to compute the left and right number fluxes for each continuum grid point *except* for the grid points adjacent to the particle region. For those points, the number flux recorded during the particles’ motion is used instead of  $F^-$ . The number density on the continuum grid is computed using (10), which is equivalent to using (14) for noninterface grid points. This completes one time step for the hybrid.

Notice that because the particle region and discretized continuum regions use the same time step and because the former is updated before the latter, no separate synchronization (i.e., ‘‘refluxing’’) is required at the end of a time step. The algorithm can also be formulated using different time steps; the region using the larger time step (typically the continuum calculation) is evaluated first, and refluxing (i.e., correcting the density according to the actual flux across the interface) is performed when the two parts are synchronized [9].

Both stochastic and nonstochastic (i.e., deterministic) PDE solvers are tested. In the former, the noise amplitude is computed using the *instantaneous* value of the local density; in the latter,  $A_{i;n} = 0$ . The deterministic method is similar to that used in particle/continuum hybrids for fluid mechanics (e.g., the DSMC/Euler hybrid in [9]).

Two types of boundary conditions are used in our simulations: periodic and Dirichlet. In the former, the points  $x = 0$  and  $x = L$  are equivalent (e.g.,  $F_1^- = F_M^+$ ) and the system is closed so  $\sum_i^M \rho_{i;n} = N/L$  is constant. With Dirichlet boundary conditions,  $\rho_{1;n}$  and  $\rho_{M;n}$  have fixed (mean) values. If either of these cells is within the particle region, then the cell is reinitialized with a number of particles selected randomly from a Poisson distribution with means  $\rho_{1;n}$  and  $\rho_{M;n}$ , respectively. The particles are then distributed in the same fashion as in the handshaking region. If the density is fixed at a boundary grid point in the stochastic PDE region, then the density at each time step is drawn from a Poisson distribution with the appropriate mean value.

## 5. SIMULATION RESULTS

### 5.1. Open, Equilibrium System

The first test case is an open system in equilibrium. Specifically, we have Dirichlet boundary conditions with (mean) density  $\rho_0$  at the endpoints. The deterministic steady state is taken as the initial condition so  $\rho_{i;1} = \bar{\rho}_{i;n} = \rho_0$ . Figures 2 and 3 show the mean density as a function of space for the particle/stochastic-PDE and, particle/deterministic-PDE hybrids, respectively. For both cases  $\Delta x = 0.5$ ,  $M = 40$ ,  $\Delta t = 0.001$ ,  $\rho_0 = 40$ , and the diffusion constant  $D = 1.0$ . From  $x = 0$  to  $x = L/2$  there are independent random walkers and from  $x = L/2$  to  $x = L$  the diffusion equation is computed on a grid of 20 cells. Our statistics are long-time averages over 10 independent samples. In both cases, the mean value of the density agrees with the expected value  $\langle \rho_{i;n} \rangle = \rho_0$ .

The stochastic and deterministic hybrids give different results for the spatial dependence of the variance, as seen in Figs. 4 and 5. The stochastic hybrid is within statistical errors of the expected value of the variance,  $\langle \delta \rho_{i;n}^2 \rangle = \rho_0 / \Delta x$  (i.e., Poisson distribution). In the deterministic hybrid, the variance is close to zero in the continuum region while in the particle region it is significantly reduced in the cells near the interface. Note that for both the deterministic- and stochastic-PDE hybrids the fluctuations in the cells near the Dirichlet boundary (where  $\rho_{1;n}$  is fixed) are *not* reduced.

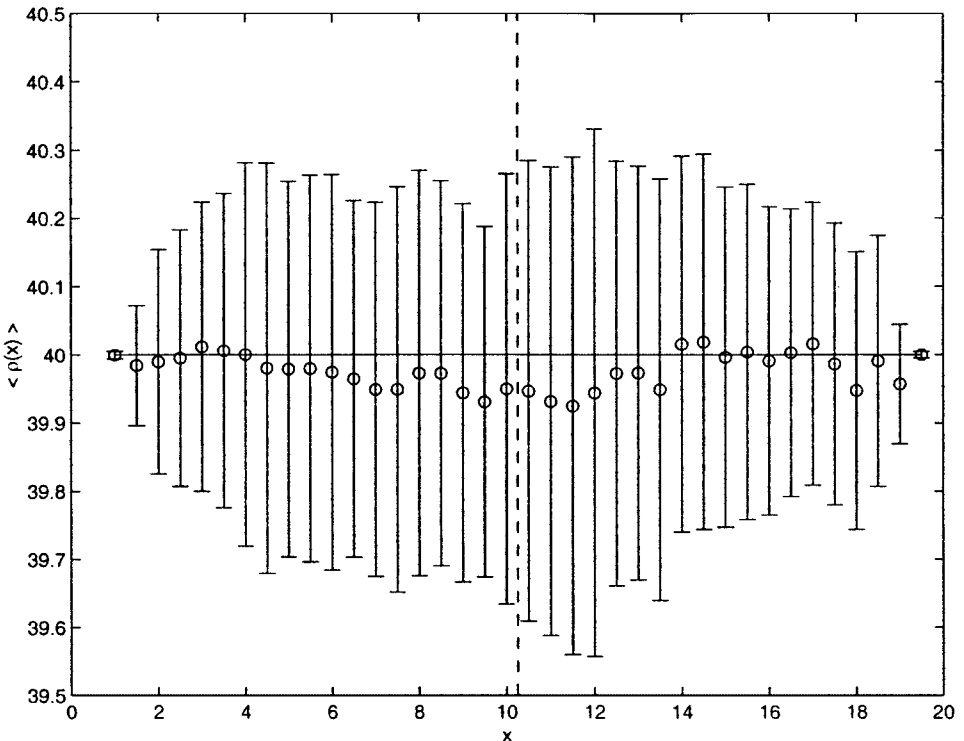


**FIG. 2.** Mean density,  $\langle \rho_{i;n} \rangle$ , for the open, equilibrium system. Circles with error bars are the data from the particle/stochastic-PDE hybrid; solid line is  $\langle \rho_{i;n} \rangle = \rho_0$ ; dashed line indicates particle/PDE interface.

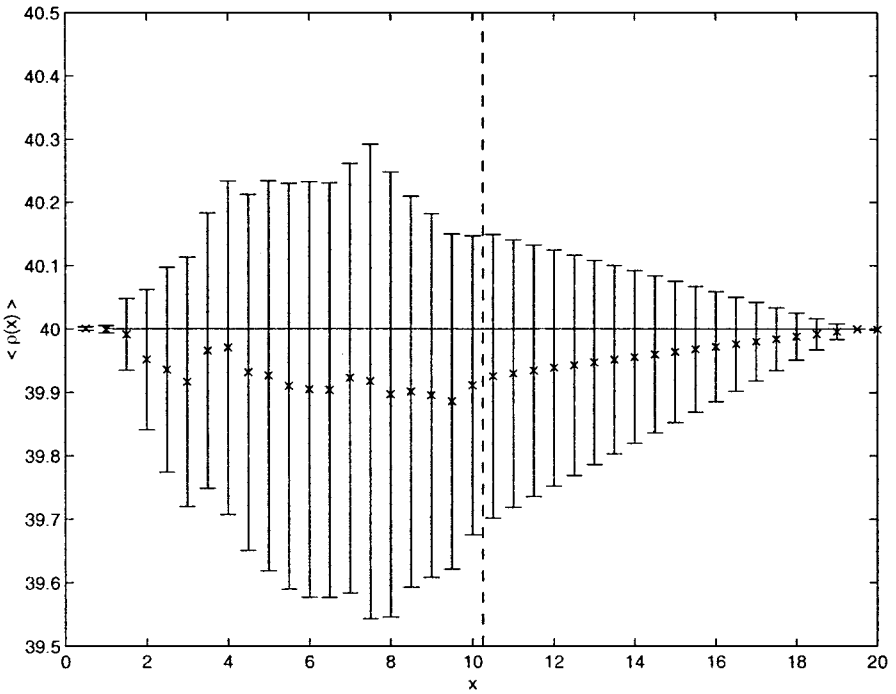


**FIG. 3.** Mean density,  $\langle \rho_{i;n} \rangle$ , for the open, equilibrium system. X-marks with error bars are the data from the particle/deterministic-PDE hybrid; solid line is  $\langle \rho_{i;n} \rangle = \rho_0$ ; dashed line indicates particle/PDE interface.

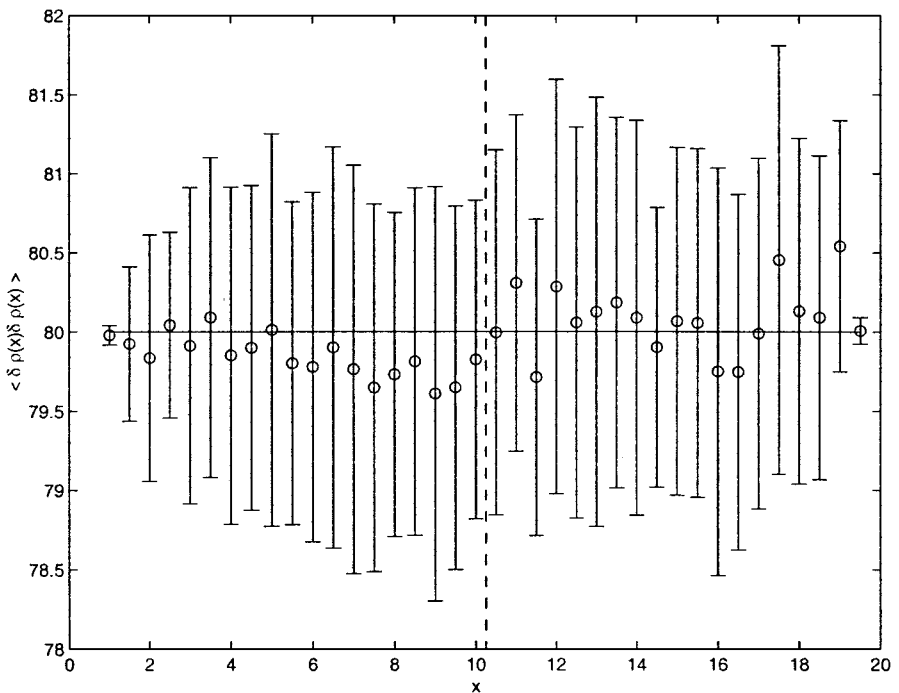


**FIG. 4.** Variance of density in a cell,  $G_{i,i} = \langle \delta \rho_{i;n}^2 \rangle$ , for the open, equilibrium system. Circles with error bars are the data from the particle/stochastic-PDE hybrid; solid line is  $\langle \delta \rho_{i;n}^2 \rangle = \rho_0 / \Delta x$ ; dashed line indicates particle/PDE interface.

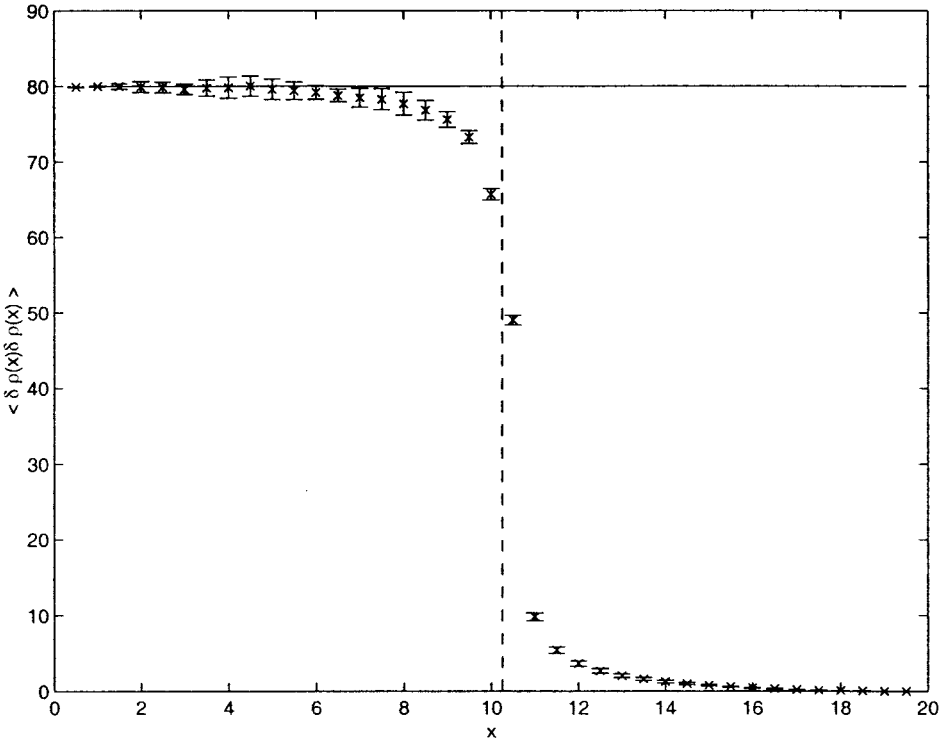


**FIG. 5.** Variance of density in a cell,  $G_{i,i} = \langle \delta \rho_{i;n}^2 \rangle$ , for the open, equilibrium system. X-marks with error bars are the data from the particle/deterministic-PDE hybrid; solid line is  $\langle \delta \rho_{i;n}^2 \rangle = \rho_0 / \Delta x$ ; dashed line indicates particle/PDE interface.

## 5.2. Closed, Equilibrium System

The second test case is a closed system in equilibrium; the computation is the same as for the open system described above except that periodic boundary conditions are used at  $x = 0$  and  $L$ . The particle/stochastic-PDE and particle/deterministic-PDE hybrids give similar results for the mean density and are in agreement with the expected value  $\langle \rho_{i;n} \rangle = \rho_0$  but give different results for the variance. The variance measured in the stochastic hybrid is in good agreement with the expected value,  $\langle \delta \rho_{i;n}^2 \rangle = \rho_0 / \Delta x - \rho_0 / L$  (see Fig. 6). Note that the variance in the closed system is reduced due to mass conservation by a factor of  $(M - 1) / M$ , and this effect is observed correctly in the hybrid because the scheme conserves mass exactly. The variance in the particle region of the deterministic hybrid is significantly reduced near the interface and goes quickly to zero within the continuum region, as shown in Fig. 7.

## 5.3. Open, Steady-State, Nonequilibrium System

The third test case is a system in which a (constant) density gradient is maintained. We take Dirichlet boundary conditions, but with different (reservoir) densities at the endpoints;  $\rho_{1,n} = \rho_0$ , and  $\rho_{M,n} = \rho_L$ . The system is initialized with the linear density profile,  $\rho_{i,1} = \rho_0 + (\rho_L - \rho_0)(i - 1) / (M - 1)$ , which is the steady state,  $\bar{\rho}_i$ . (This initialization leads to faster convergence of statistics; any other would lead to the correct steady state.) Both particle/stochastic-PDE and particle/deterministic-PDE hybrids were tested. Again,

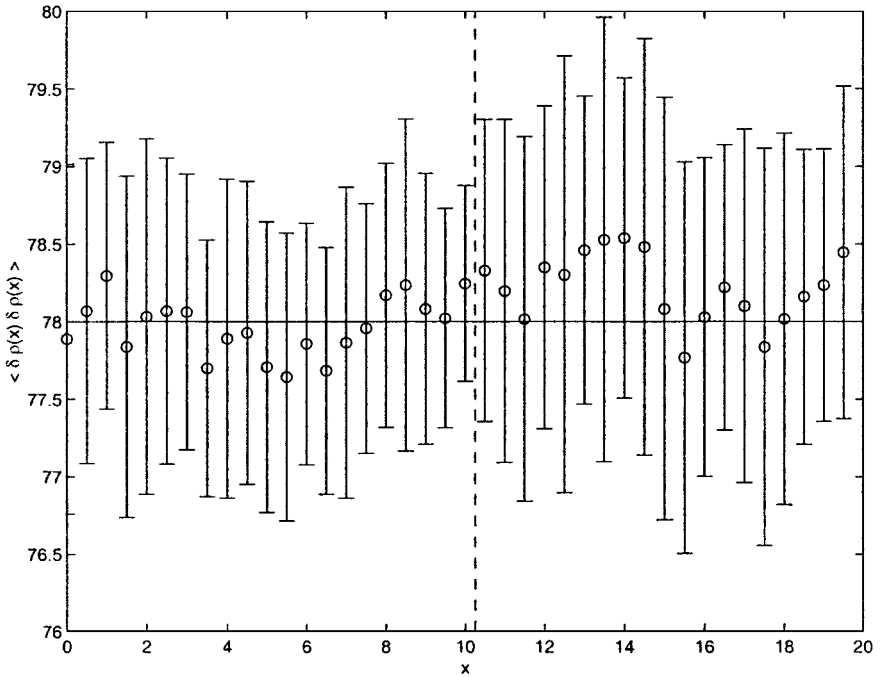


**FIG. 6.** Variance of density in a cell,  $G_{i,i} = \langle \delta \rho_{i,n}^2 \rangle$ , for the closed, equilibrium system. Circles with error bars are the data from the particle/stochastic-PDE hybrid; solid line is  $\langle \delta \rho_{i,n}^2 \rangle = \rho_0 / \Delta x - \rho_0 / L$ ; dashed line indicates particle/PDE interface.

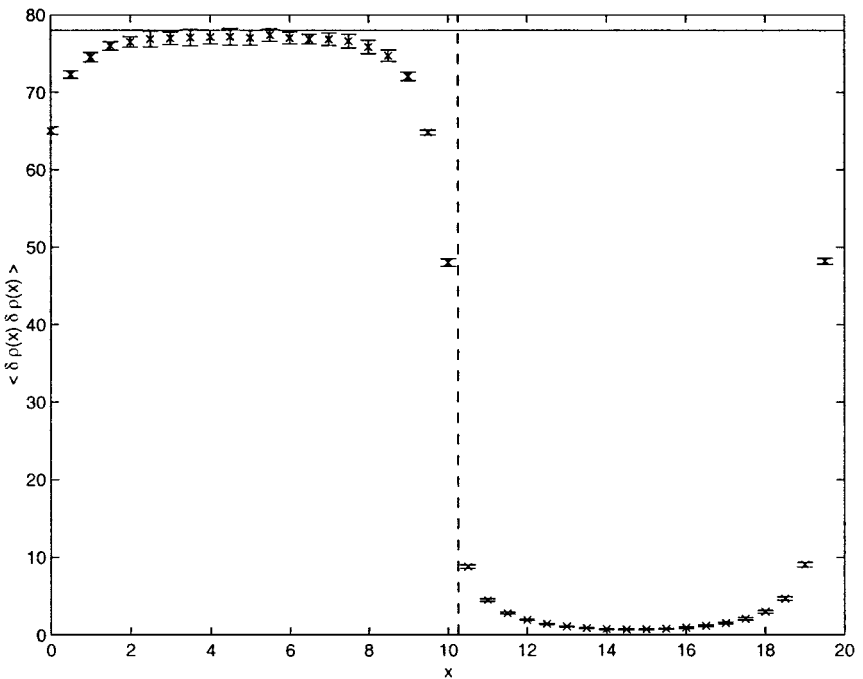


**FIG. 7.** Variance of density in a cell,  $G_{i,i} = \langle \delta \rho_{i,n}^2 \rangle$ , for the closed, equilibrium system. X-marks with error bars are the data from the particle/deterministic-PDE hybrid; solid line is  $\langle \delta \rho_{i,n}^2 \rangle = \rho_0 / \Delta x - \rho_0 / L$ ; dashed line indicates particle/PDE interface.

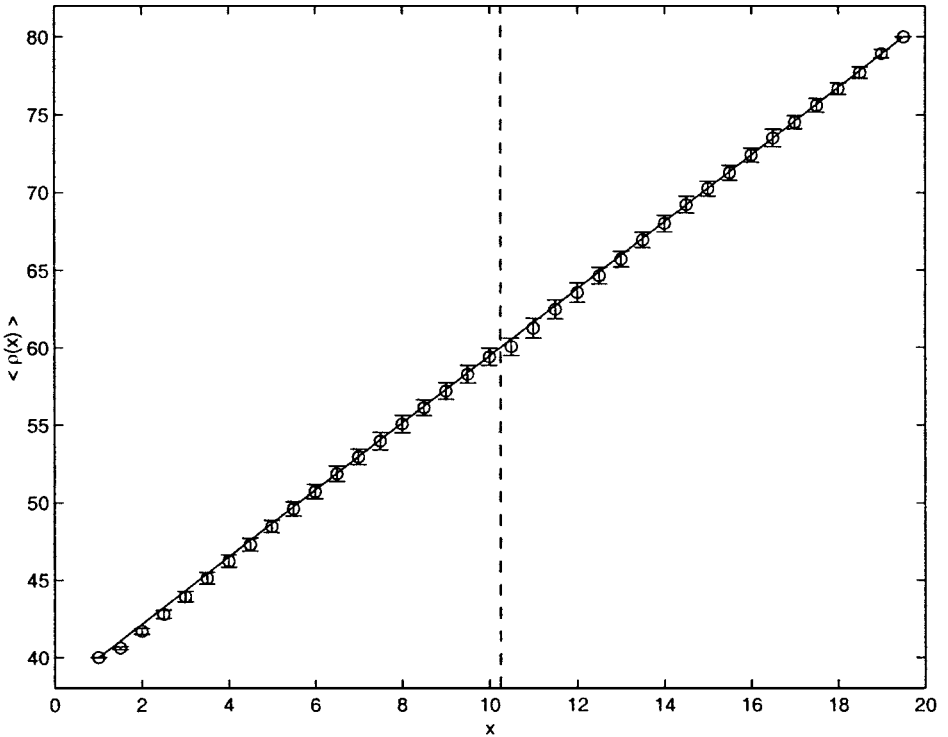


**FIG. 8.** Mean density,  $\langle \rho_{i;n} \rangle$ , for the open, nonequilibrium system. Circles with error bars are the data from the particle/stochastic-PDE hybrid; solid line is  $\langle \rho_{i;n} \rangle = \bar{\rho}_i$ ; dashed line indicates particle/PDE interface.

for both cases  $\Delta x = 0.5$ ,  $\Delta t = 0.001$ , and the diffusion constant,  $D = 1.0$ ; densities at the endpoints were  $\rho_0 = 40$ ,  $M = 40$ , and  $\rho_L = 80$ . From  $x = 0$  to  $x = L/2$  there are independent random walkers, and from  $x = L/2$  to  $x = L$  the diffusion equation is computed on a grid of 20 cells. As before, in the stochastic case, for the noise amplitude we use the *instantaneous* value of the local density.

Figures 8 and 9 show the mean density as a function of position for the hybrids using the stochastic and deterministic PDE solvers, respectively. Our statistics are long-time averages over 10 independent samples. In both cases, the mean value of the density agrees with the expected value of  $\langle \rho_{i;n} \rangle = \bar{\rho}_i$ , which is linear in  $x$ . For the stochastic hybrid the variance is within statistical errors of its exact value,  $\langle \delta \rho_{i;n}^2 \rangle = \bar{\rho}_i / \Delta x$  (see Fig. 10). The variance in the particle region of the nonstochastic hybrid is significantly reduced near the interface and goes quickly to zero within the continuum region, as shown in Fig. 11.

#### 5.4. Time-Dependent System

The final test case investigates the ability of the hybrid to capture time-dependent phenomena. In particular, we investigate a system initially with a uniform average density  $\rho_0$  upon which is superimposed a delta function spike of amplitude  $N_s$  at  $x_0$ . In this case we prescribe Dirichlet boundary conditions, fixing the density to  $\rho_0$  at  $x = 0$  and  $L$ . The spike is placed within the particle region so at  $t = 0$  there are  $N_s$  particles at  $x = x_0$ . As time

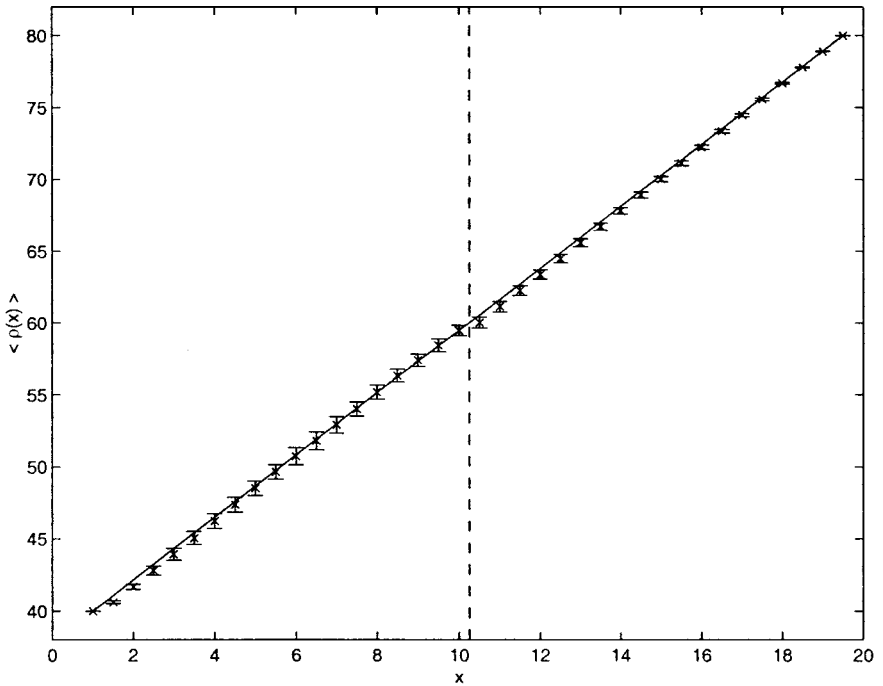


**FIG. 9.** Mean density,  $\langle \rho_{i;n} \rangle$ , for the open, nonequilibrium system. X-marks with error bars are the data from the particle/deterministic-PDE hybrid; solid line is  $\langle \rho_{i;n} \rangle = \bar{\rho}_i$ ; dashed line indicates particle/PDE interface.

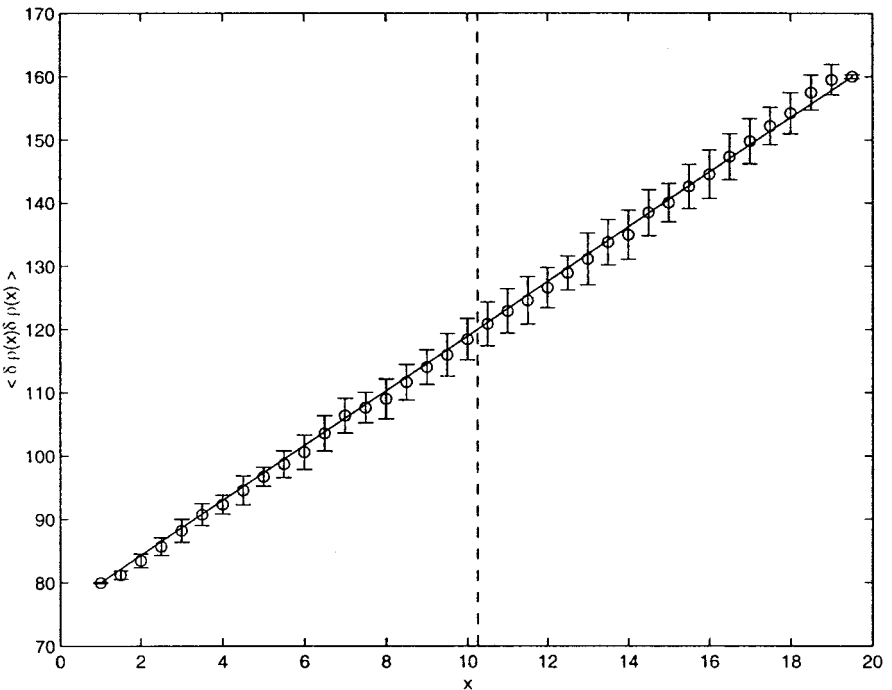


**FIG. 10.** Variance of density in a cell,  $G_{i,i} = \langle \delta \rho_{i;n}^2 \rangle$ , for the open, nonequilibrium system. Circles with error bars are the data from the particle/stochastic-PDE hybrid; solid line is  $\langle \delta \rho_{i;n}^2 \rangle = \bar{\rho}_i / \Delta x$ ; dashed line indicates particle/PDE interface.

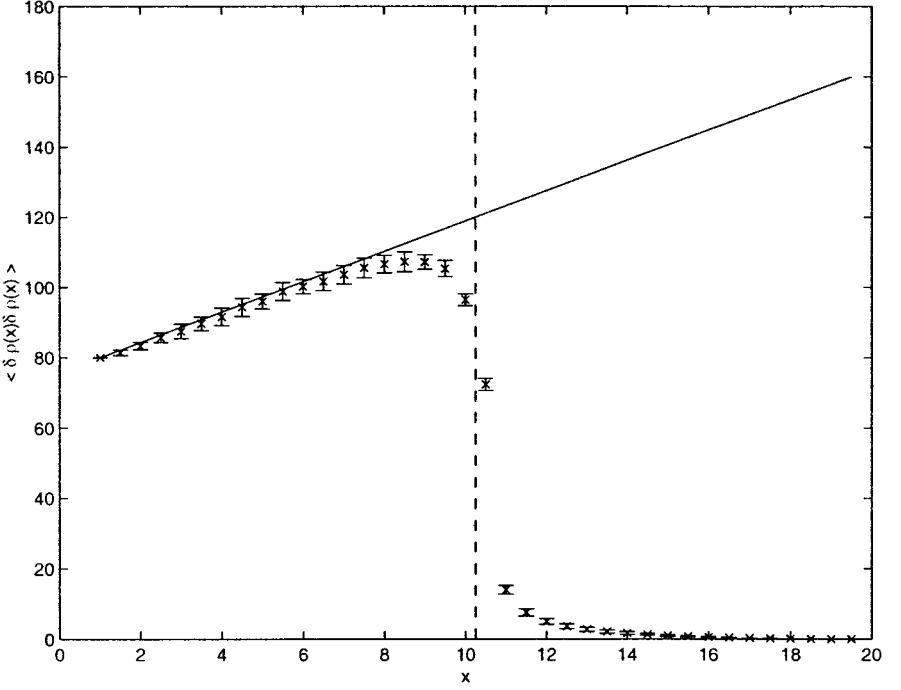


**FIG. 11.** Variance of density in a cell,  $G_{i,i} = \langle \delta \rho_{i;n}^2 \rangle$ , for the open, nonequilibrium system. X-marks with error bars are the data from the particle/deterministic-PDE hybrid; solid line is  $\langle \delta \rho_{i;n}^2 \rangle = \bar{\rho}_i / \Delta x$ ; dashed line indicates particle/PDE interface.

progresses, the spike decays and by the method of images,

$$\langle \rho(x, t) \rangle = \rho_0 + N_s \sum_{j=-\infty}^{\infty} \mathcal{G}(x - x_j^s, t), \quad (19)$$

where  $x_j^s = (-1)^j x_0 + (j + \frac{1}{2} + (-1)^{j+1} \frac{1}{2})L$  is the location of the spike and its images, and

$$\mathcal{G}(x, t) = \frac{1}{\sqrt{4\pi Dt}} e^{-x^2/(4Dt)} \quad (20)$$

is the Green's function for the infinite system. The sum of images is required by the Dirichlet boundary conditions but for short times ( $t \ll L^2/D$ ), the solution is well approximated by just the  $j = 0$  term.

The expected mean density is

$$\langle \rho_{i;n} \rangle = \frac{N_s}{\Delta x} v_{i;n} + \rho_0, \quad (21)$$

and the time-dependent density variance within a cell of size  $\Delta x$  is

$$\langle \delta \rho_{i;n}^2 \rangle = \frac{N_s}{\Delta x^2} v_{i;n} (1 - v_{i;n}) + \frac{\rho_0}{\Delta x} = \frac{\langle \rho_{i;n} \rangle}{\Delta x} - \frac{N_s}{\Delta x^2} v_{i;n}^2, \quad (22)$$

where  $v_{i;n}$  is the probability of a particle, initially in the spike (or one of its images), moving

into cell  $i$  for which  $x_i - \frac{1}{2}\Delta x \leq x' \leq x_i + \frac{1}{2}\Delta x$  and is given by

$$v_{i;n} = \sum_{j=-\infty}^{\infty} \int_{x_i - \frac{1}{2}\Delta x}^{x_i + \frac{1}{2}\Delta x} \mathcal{G}(x' - x_j^s, n\Delta t) dx' \quad (23)$$

$$\approx \int_{x_i - \frac{1}{2}\Delta x}^{x_i + \frac{1}{2}\Delta x} \mathcal{G}(x' - x_0, n\Delta t) dx', \quad (24)$$

for  $t \ll L/D$ . Note that this formulation of the variance, using the random walk stochastic process, yields a variance that is *not* Poissonian, that is, with  $\langle \delta\rho_{i;n}^2 \rangle \neq \bar{\rho}_{i;n}/\Delta x$ .

The system is initialized with the uniform density profile,  $\rho_{i;1} = \rho_0$ , plus a fixed number of particles,  $N_s = 20$ , placed initially at the point  $x_0 = 8.25$ ; which is the center of cell  $i = 17$ . Both particle/stochastic and particle/deterministic PDE hybrids were tested. The system parameters are the same as in the above examples, namely,  $\Delta x = 0.5$ , and  $\Delta t = 0.001$ . From  $x = 0$  to  $x = L/2$  there are independent random walkers and from  $x = L/2$  to  $x = L$  the diffusion equation is computed on a grid of 20 cells. As before, in the stochastic case, for the noise amplitude we use the *instantaneous* value of the local density.

Figures 12 and 13 show the mean density as a function of space. Our statistics are averages over 40,000 independent samples. To test the validity of the hybrid, we choose a time,  $t = 0.8$ , which satisfies the condition  $t \ll L^2/D = 400$ . More importantly, the time is long enough to have a significant portion of the pulse decaying into the continuum region, leading to a time-dependent gradient across the interface. In both the stochastic and deterministic cases, the mean value of the density agrees with the expected value of  $\langle \rho_{i;n} \rangle$  given by Eq. (21). For

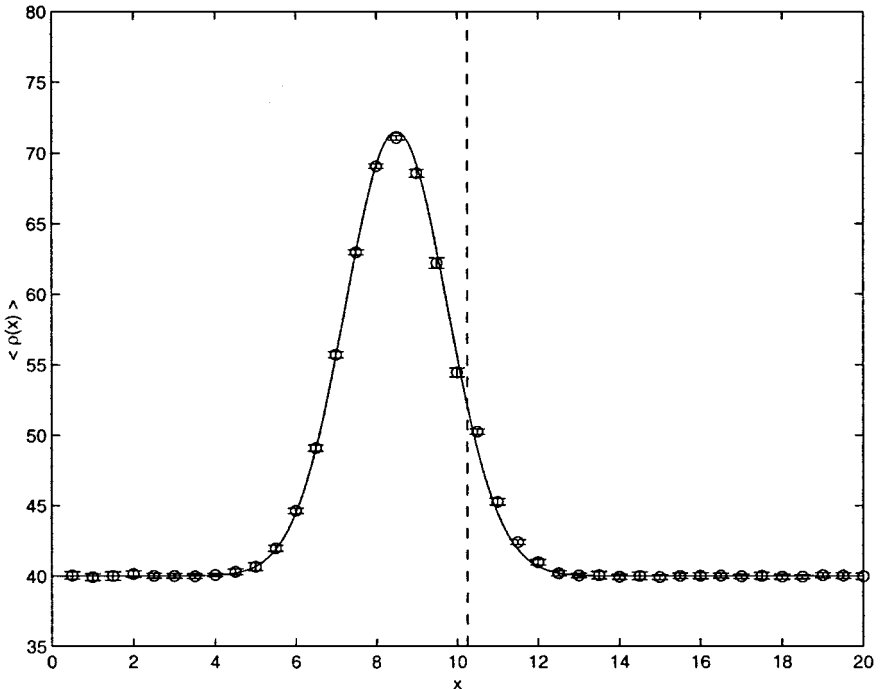


**FIG. 12.** Time-dependent mean density,  $\langle \rho_{i;n} \rangle$ , for the decaying pulse. Circles with error bars are the data from the particle/stochastic-PDE hybrid; solid line is given by (21); dashed line indicates particle/PDE interface.

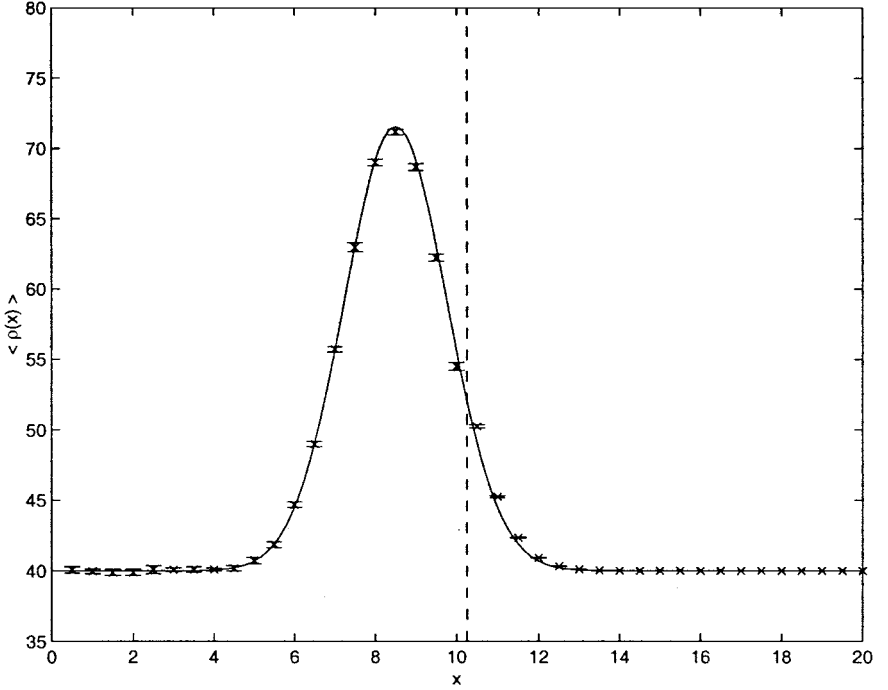


**FIG. 13.** Time-dependent mean density,  $\langle \rho_{i;n} \rangle$ , for the decaying pulse. X-marks with error bars are the data from the particle/deterministic-PDE hybrid; solid line is given by (21); dashed line indicates particle/PDE interface.

the stochastic hybrid (Fig. 14) the variance is within statistical errors of its exact value. But again, the variance in the particle region of the deterministic hybrid (Fig. 15) is significantly reduced near the interface and goes quickly to zero in the continuum region.

## 6. ANALYTICAL RESULTS FOR STEADY-STATE VARIANCE

The various cases examined in the previous section reveal that the deterministic version of the particle/continuum hybrid (i.e., without the stochastic flux) gives the correct mean density but not the right variance. Specifically, the variance in the particle region of the deterministic hybrid is significantly reduced near the interface and decays quickly to zero in the continuum region (see Figs. 5, 7, 11, and 15). In this section we introduce an approximate model that reproduces this effect.

Consider the discretized Langevin scheme for the fluctuating diffusion equation (see Eq. (14)),

$$\begin{aligned} \rho_{i;n+1} = & \rho_{i;n} + \frac{D\Delta t}{\Delta x^2} (\rho_{i+1;n} + \rho_{i-1;n} - 2\rho_{i;n}) \\ & - \sqrt{\frac{\Delta t}{2\Delta x^3}} (\sqrt{A_{i;n} + A_{i+1;n}} \mathfrak{R}_{i;n} - \sqrt{A_{i;n} + A_{i-1;n}} \mathfrak{R}_{i-1;n}). \end{aligned} \quad (25)$$

In this section we analyze a model for which

$$A_{i;n} = \begin{cases} 2D\bar{\rho}_{i;n} & i \leq M/2 \\ 0 & \text{otherwise.} \end{cases} \quad (26)$$

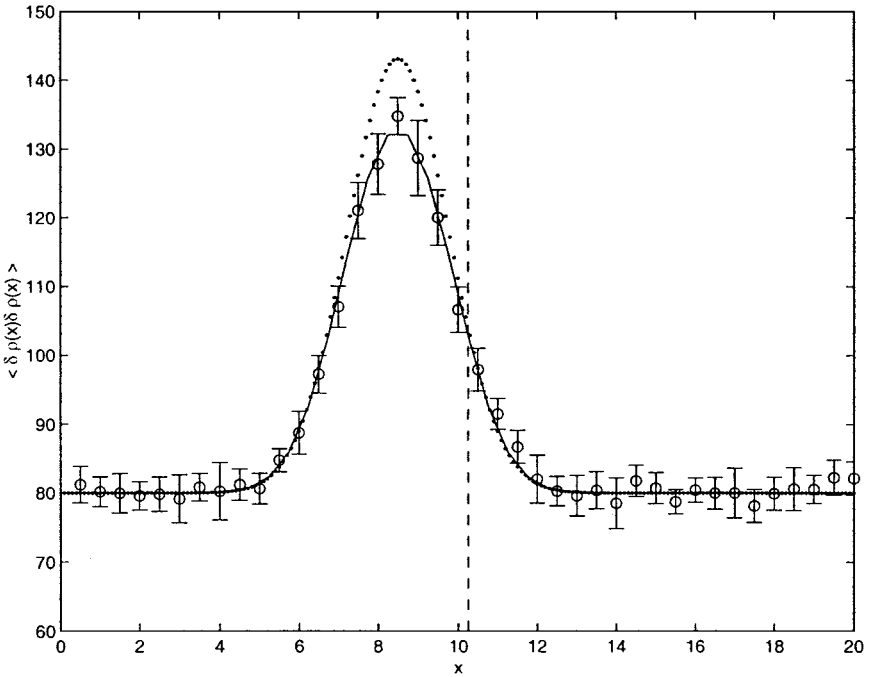


**FIG. 14.** Time-dependent density variance,  $G_{i,i} = \langle \delta \rho_{i,n}^2 \rangle$ , for the decaying pulse. Circles with error bars are the data from the particle/stochastic-PDE hybrid; solid line is given by (22); dotted line is  $\langle \delta \rho_{i,n}^2 \rangle = \langle \rho_{i,n} \rangle / \Delta x$ ; dashed line indicates particle/PDE interface.

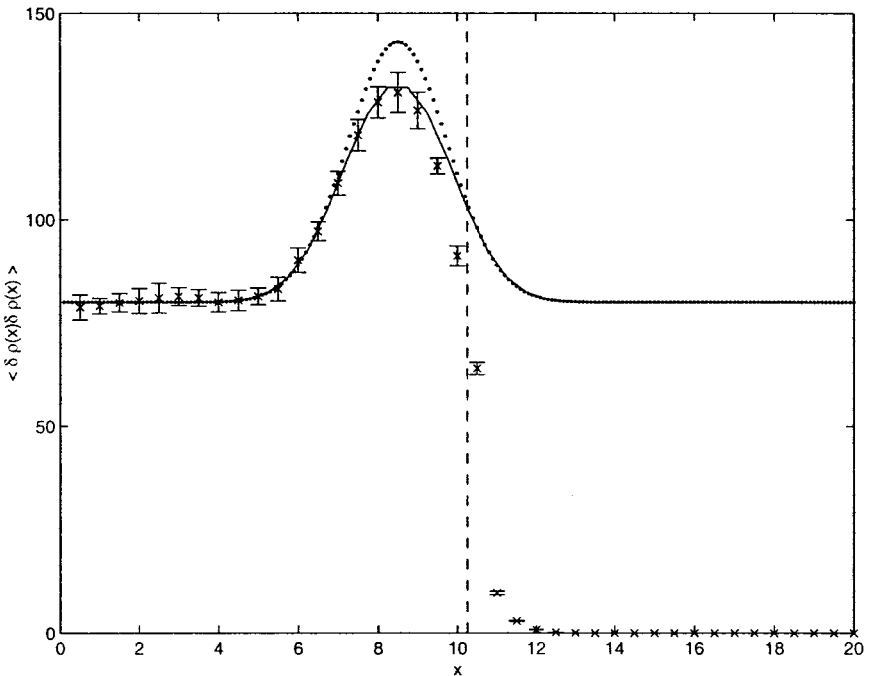


**FIG. 15.** Time-dependent density variance,  $G_{i,i} = \langle \delta \rho_{i,n}^2 \rangle$ , for the decaying pulse. X-marks with error bars are the data from the particle/deterministic-PDE hybrid; solid line is given by (22); dotted line is  $\langle \delta \rho_{i,n}^2 \rangle = \langle \rho_{i,n} \rangle / \Delta x$ ; dashed line indicates particle/PDE interface.

That is, the noise amplitude is zero for the cells in the right half of the system. We will refer to this as a “half-stochastic” PDE solver.

This half-stochastic model is equivalent to a hybrid that combines a stochastic PDE solver with a nonstochastic PDE solver. The fluctuations in this model are *qualitatively* similar to those in a particle/deterministic PDE hybrid, with the stochastic PDE solver mimicking the particle computation. The model is not equivalent to a particle/deterministic PDE hybrid because the fluctuating particle flux for random walkers is not a white noise process. Nevertheless, this model is ideally suited for testing the effects of noise, since we are coupling two systems of the same type (both PDE solvers).

By construction, the half-stochastic model gives the same mean density as a deterministic PDE solver, that is,  $\langle \rho_{i;n} \rangle = \bar{\rho}_{i;n}$ . The equal-time correlation function,  $G_{i,j}$ , for this model is given by Eq. (15) with

$$B_i = \begin{cases} \sqrt{\bar{\rho}_{i;n} + \bar{\rho}_{i+1;n}} & i < M/2 \\ \sqrt{\bar{\rho}_{i;n}} & i = M/2 \\ 0 & \text{otherwise,} \end{cases} \quad (27)$$

and Eq. (15) easily may be solved numerically (e.g., by relaxation [18]).

We again consider the first test case discussed in the previous section: an open system at equilibrium. Recall that the density at the end points is fixed to  $\rho_{1;n} = \rho_{M;n} = \rho_0$  with  $\rho_0 = 40$ . For an open system, the variance at equilibrium should equal  $\langle \delta \rho_{i;n}^2 \rangle = \rho_0 / \Delta x = 80$ . Solving (15) using (27) gives the results shown in Fig. 16; this result was verified using a

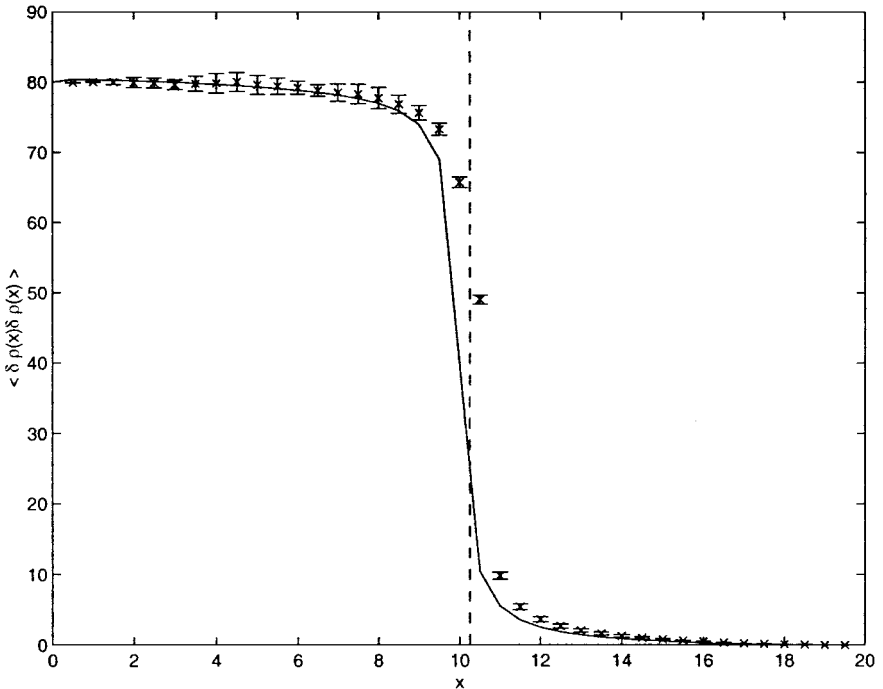


**FIG. 16.** Density variance,  $G_{i,i} = \langle \delta \rho_{i;n}^2 \rangle$ , in an open system at equilibrium for the half-stochastic PDE model (solid line) and the particle/nonstochastic PDE hybrid (points; same as Fig. 5); dashed line indicates the interface.

stochastic-PDE/deterministic-PDE hybrid and perfect agreement was found. As discussed above, the half-stochastic model is qualitatively similar to a particle/deterministic-PDE hybrid, which is seen in Fig. 16, where the results from such a hybrid are also shown. Similar results are found when we compare the half-stochastic model with the deterministic hybrid for the other cases presented in the previous section. Given that such half-stochastic models are much simpler than the discrete/continuous stochastic process underlying the construction of a deterministic hybrid, we believe that they will be very useful in the study of other particle/continuum hybrids.

## 7. CONCLUDING REMARKS

Our aim in this study was to determine if particle/continuum hybrids, such as those used in Algorithm Refinement, could accurately model hydrodynamic fluctuations. Our results show that such hybrids, constructed to solve the linear diffusion PDE and the random walk particle model, are capable of capturing *some* fluctuations correctly for equal-time equilibrium, nonequilibrium steady-state, and time-dependent problems. We find that the mean density is given correctly by particle/PDE hybrids using either stochastic or deterministic PDE solvers. The variance can be recovered everywhere with a particle/stochastic-PDE hybrid but is only correct within the particle region far from the coupling interface when the continuum solver does not contain stochastic fluxes. This reduction of the density variance in the particle region when coupled with a deterministic PDE necessitates placing the interface further away from regions where accurate fluctuations are required. If such measures are not taken, we believe this can have a deleterious effect when using a deterministic PDE solver in hybrids that simulate strongly interacting systems (e.g., nonequilibrium solids and dense liquids).

It is important to note that the linear diffusion equation is a particularly simple PDE, and while the results presented here are encouraging, one should not assume that particle/continuum hybrids will do equally well for other physical systems. For simple fluids, the extension of the present formulation to the stochastic PDEs of linearized fluctuating hydrodynamics is straightforward [14, 19]. Furthermore, different hybrid coupling schemes will have different effects on the fluctuations, even for the linear diffusion equation [20].

For highly nonlinear equations or for systems with more general multiplicative noises, deterministic hybrids can have mean values that differ across the coupling interface, even in equilibrium. In these cases great care must be taken in the construction of the hybrid; renormalized noises or effective potentials (from which the PDE is derived) may prove useful. This is likely to play an important role in nonlinear time-dependent Ginzburg–Landau models of solids and is currently under investigation. It will be interesting to consider models such as those in the previous section (stochastic-PDE/deterministic-PDE hybrid) for nonlinear equations. Results found in these models should be qualitatively similar to those for particle/deterministic PDE hybrids, but the theoretical and numerical studies are easier to perform.

In our study of fluctuations in simple diffusion we focused our attention on the variance of density, but for other physical systems equal-time correlations are also of interest. A common feature found in the stochastic PDEs arising from fluctuating hydrodynamics is the existence of long-range correlations of equal-time fluctuations at nonequilibrium steady states [21]. The linear diffusion equation for density, however, does *not* have such

long-range correlations (although we find them in the linear Fourier equation [14]). For systems with long-range correlations we expect that the influence of the continuum solver on the fluctuations in the particle region will be enhanced; we are currently conducting a study of hybrids for such systems.

Clearly, any macroscopic formulation will have limited fidelity to the underlying microscopic processes. Stochastic PDEs of physical processes are typically formulated to guarantee *only* the correct single-time fluctuations. For example, in fluctuating hydrodynamics the amplitude of the noise is fixed by matching the variances at thermodynamic equilibrium [19]. The inability to capture even single-time current fluctuations (a higher order moment) is already observed in the linear diffusion equation. To reproduce such statistics a more complex formulation, such as extended irreversible thermodynamics, may be needed. A related question is whether time-correlations of fluctuations can be recovered, even with a stochastic-PDE hybrid; we are currently exploring this issue.

While the advantages of a particle/continuum hybrid are evident, unfortunately, for some physical systems either an accurate microscopic particle algorithm is available or a stochastic macroscopic model is known, but not both. Even when both elements are available, the two methods may not be compatible for coupling together. The construction of hybrids is particularly challenging for these systems.

Though we find that a hybrid scheme constructed with a simple, explicit stochastic-PDE solver can reproduce the correct fluctuations, it is not our intent to promote the present scheme as being optimal. A topic for future study is the analysis of a variety of stochastic-PDE schemes to establish the most accurate and efficient methods for particle/continuum hybrids. In particular, the details of how the coupling is implemented may affect the convergence properties of a hybrid.

In this paper we consider explicit schemes because these are the most commonly used methods for the continuum calculations in hybrids. Elliptic PDEs, such as the diffusion equation, are often solved by implicit methods (e.g., Crank–Nicolson). Because such schemes introduce a nonlocal coupling, the modification to the fluctuations may be significant especially in hybrids using deterministic-PDEs. While semi-implicit PDE solvers have been used in particle/continuum hybrids [9], the study of implicit, stochastic hybrids is a topic best treated in a separate paper.

Finally, we have not addressed the question of how one selects the regions in a calculation that should be computed by a microscopic, particle scheme versus a macroscopic, continuum method. For example, when a hybrid is fully “adaptive” the particle regions can grow, shrink, shift, merge, and fission throughout the calculational domain. In adaptive mesh refinement, gradient detection is a commonly used refinement criterion (e.g., using a fine grid near a shock front). Spontaneous fluctuations in a stochastic or particle-based algorithm can trigger such criteria, even in regions that are at thermodynamic equilibrium, causing unnecessary refinement. Preliminary studies using an adaptive DSMC/Euler hybrid indicate that this problem may be overcome by a judicious choice of multiple refinement criteria [22], but this important computational issue merits further study.

## ACKNOWLEDGMENTS

The authors thank B. Alder, G. L. Eyink, R. Hornung, M. Malek-Mansour, K. Pao, and C. van den Broeck for helpful discussions. This work was performed under the auspices of the U.S. Department of Energy by University of California Lawrence Livermore National Laboratory under Contract W-7405-Eng-48; at LANL

(LA-UR 01-5767) by LDRD-DR-2001501 and the Program in Applied Mathematical Sciences Contract KC-07-01-01, and at Boston University by NSF-KDI 987333.

## REFERENCES

1. D. C. Wadsworth and D. A. Erwin, One-Dimensional hybrid continuum/particle simulation approach for rarefied hypersonic flows, *AIAA Paper* 90-1690 (1990).
2. F. F. Abraham, J. Q. Broughton, N. Bernstein, and E. Kaxiras, Spanning the length scales in dynamic simulation, *Comput. Phys.* **12**, 538 (1998).
3. D. Hash and H. Hassan, A decoupled DSMC/Navier-Stokes analysis of a transitional flow experiment, *AIAA Paper* 96-0353 (1996).
4. J. Bourgat, P. Le Tallec, and M. Tidriri, Coupling Boltzmann and Navier-Stokes equations by friction, *J. Comput. Phys.* **127**, 227 (1996).
5. B. J. Alder, Highly discretized dynamics, *Phys. A* **240**, 193 (1997).
6. P. Le Tallec and F. Mallinger, Coupling Boltzmann and Navier-Stokes equations by half fluxes, *J. Comput. Phys.* **136**, 51 (1997).
7. N. Hadjiconstantinou and A. Patera, Heterogeneous atomistic-continuum representations for dense fluid systems, *Int. J. Mod. Phys. C* **8**, 967 (1997).
8. S. Tiwari and A. Klar, Coupling of the Boltzmann and Euler equations with adaptive domain decomposition procedure, *J. Comput. Phys.* **144**, 710 (1998).
9. A. L. Garcia, J. B. Bell, W. Y. Crutchfield, and B. J. Alder, Adaptive mesh and algorithm refinement using direct simulation Monte Carlo, *J. Comput. Phys.* **154**, 134 (1999).
10. R. E. Rudd and J. Q. Broughton, Concurrent coupling of length scales in solid state systems, *Phys. Status Solidi B* **217**, 251 (2000).
11. E. G. Flekkoy, G. Wagner, and J. Feder, Hybrid model for combined particle and continuum dynamics, *Europhys. Lett.* **52**, 271 (2000).
12. V. B. Shenoy, R. Miller, E. B. Tadmor, D. Rodney, R. Phillips, and M. Ortiz, An adaptive finite element approach to atomic-scale mechanics—the quasicontinuum method, *J. Mech. Phys. Solids* **47**, 611 (1999).
13. C. W. Gardiner, *Handbook of Stochastic Methods*, 2nd ed. (Springer-Verlag, Berlin, 1985).
14. A. L. Garcia, M. Malek Mansour, G. Lie, and E. Clementi, Numerical Integration of the Fluctuating Hydrodynamic Equations, *J. Stat. Phys.* **47**, 209 (1987).
15. C. Z.-W. Liu and I. Oppenheim, Spatial correlations in bounded nonequilibrium fluid systems, *J. Stat. Phys.* **86**, 179 (1997).
16. A. L. Garcia, G. Sonnino, and M. Malek-Mansour, Long range correlations in simple nonequilibrium fluids, *J. Stat. Phys.* **90**, 1489 (1998).
17. N. G. van Kampen, *Stochastic Processes in Physics and Chemistry* (North-Holland, Amsterdam, 1981).
18. A. L. Garcia, *Numerical Methods for Physics* (Prentice Hall International, Upper Saddle River, NJ, 2000).
19. L. D. Landau and E. M. Lifshitz, *Fluid Mechanics* (Pergamon, Oxford, 1959).
20. E. G. Flekkoy, J. Feder, and G. Wagner, Coupling particles and fields in a diffusive hybrid model, *Phys. Rev. E* **64**, 066302 (2001).
21. R. Schmitz, Fluctuations in nonequilibrium fluids, *Phys. Rep.* **171**, 1 (1988).
22. R. Hornung, personal communication, 2001.